VI. APPENDIX

A. Supplementary figures

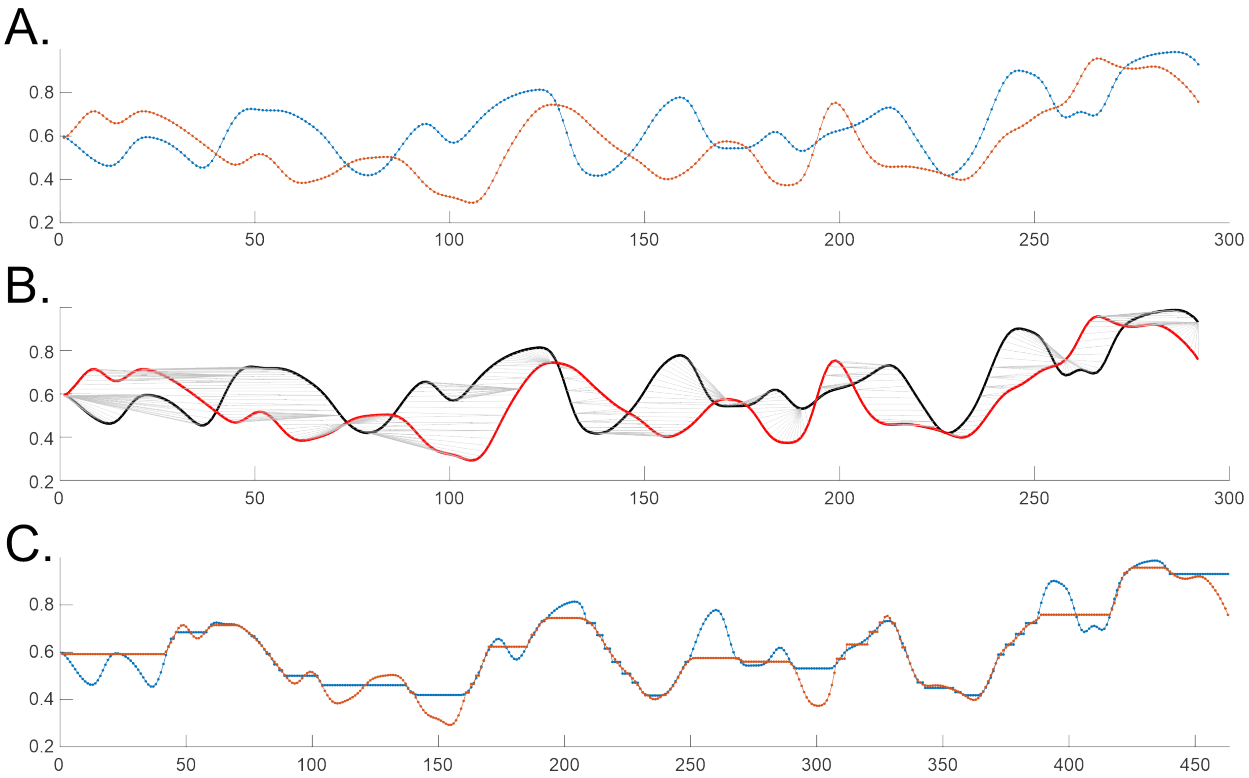

Fig. S1. **Dynamic Time Warping** (DTW) method is based on applying series of stretches that maximize alignment between two profiles at minimal cost, without omitting elements or scrambling their order. DTW is commonly used to quantify similarity between waveforms, e.g., for recognizing similar speech patterns [78], and is naturally suitable for comparing spectral waves. **A**. Two concurrent segments of the hippocampal, ν_θ^h (blue line), and the cortical, ν_θ^c (red line), spectral waves. Each segment contains about 300 data points (time-wise this amounts to about 40 ms), normalized by their respective means and shifted vertically into the $0 \lesssim y \lesssim 1$ range. **B**. Each point from ν_θ^h is matched to one or more points of ν_θ^c and vice versa, using MATLAB's dtw function. The gray lines show pairs of aligned points. One-to-many connection lines (gray) mark the stretchings. Note that different segments of spectral waves alternately lag and outpace one another: the algorithm compensates these shifts to match the shapes. **C**. After the alignments, the number of points increases by 50% (note the stretched-out x-axis). The point-by-point separation in the resulting alignment, measured in Euclidean metric and normalized to the original curve lengths serves quantifies the spectral waves' shape difference, which in this case amounts to 7%.

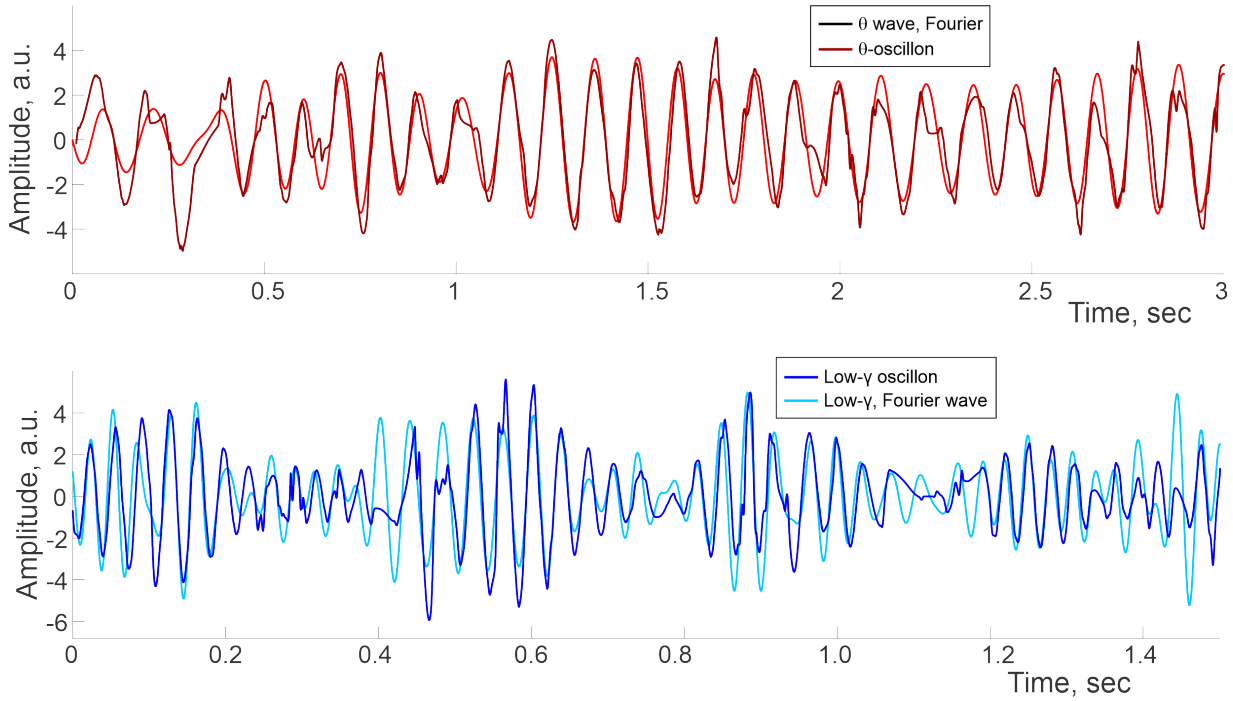

Fig. S2. **Comparative waveforms** of Fourier θ-wave ($4-12$ Hz) and θ-oscillon (top panel) and slow-γ wave, Fourier-filtered between 20 and 40 Hz, compared to slow-γ oscillon (bottom panel). Despite similar oscillation rates, the wave shapes are different.

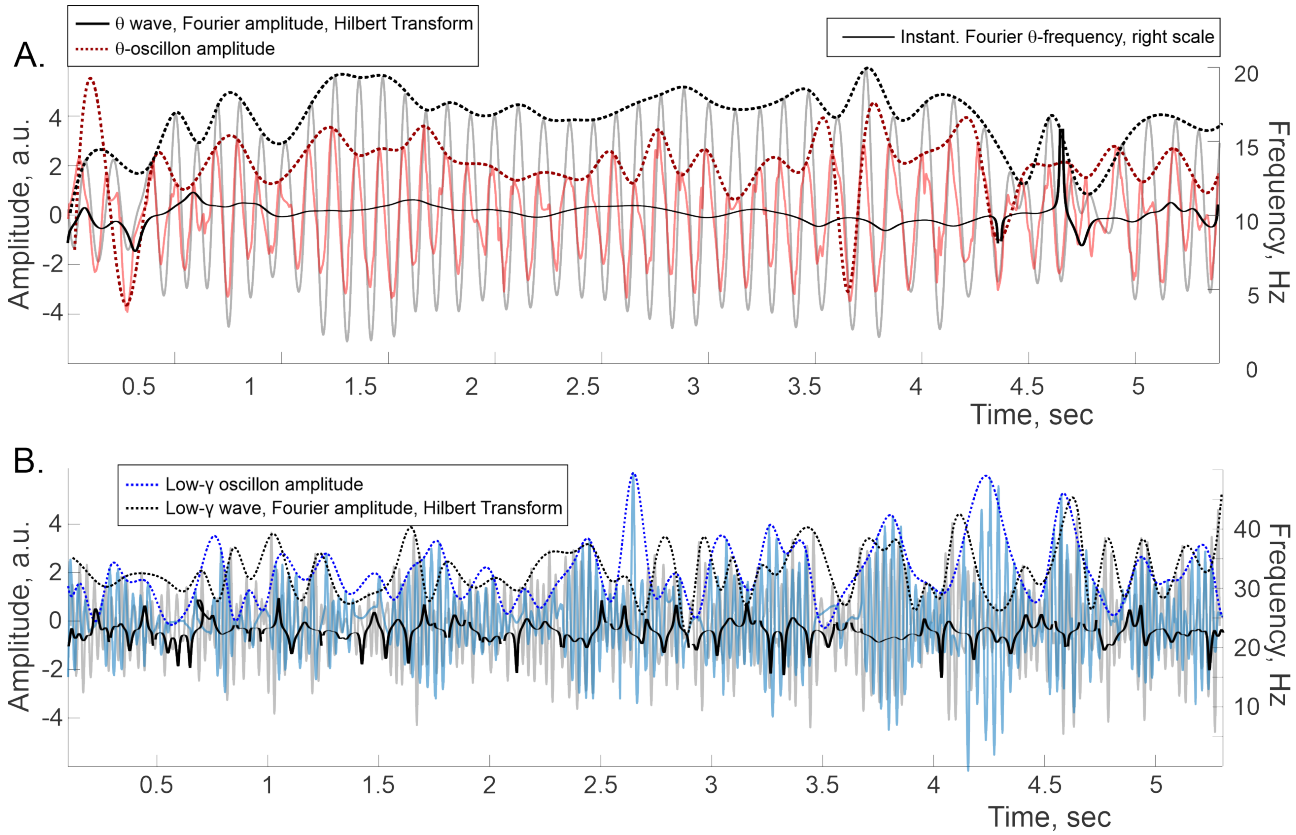

Fig. S3. **Hilbert transform**. **A**. Fourier-defined θ-wave (gray waveform in the background) shown with its amplitude (dotted line on top) and the corresponding instantaneous frequency (black line, placed according to the right scale) produced by Hilbert transform. Pink waveform in the foreground shows θ-oscillon and its amplitude computed from the net contribution of stable poles contributing to spectral wave (dotted brown line). **B**. Fourier-defined slow-γ wave (20 – 40 Hz), compared to the slow-γ oscillon. Amplitudes and frequencies are as above. The amplitude of the latter is lower because it does not include the noise component.

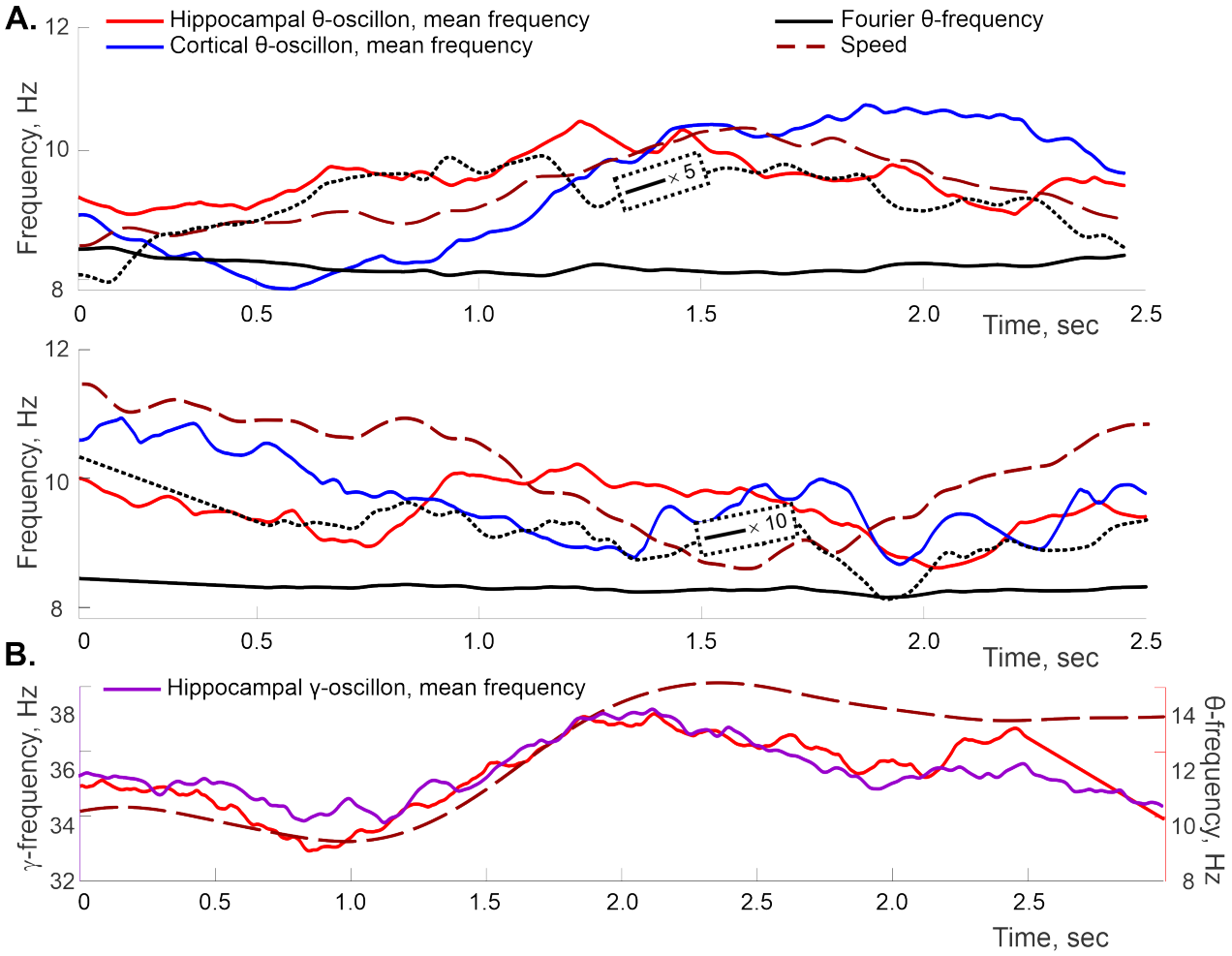

Fig. S4. **Speed vs. mean θ-frequency coupling**. **A**. Additional examples demonstrating covariance between the moving mean of the hippocampal (blue) and the cortical (red) θ-frequency with the rat's speed (dashed brown curve). The latter is scaled vertically and shifted as on Fig. 4, to match the frequency ranges. The instantaneous frequency of the traditional, Fourier-defined θ-waves is shown by solid black curve, as on Fig. 3. A five-fold (top panel) and ten-fold (bottom panel) vertical stretch of the Fourier-frequency produces the dotted black curve, whose similarity to the spectral waves' means explains the general correspondence between our results and conventional evaluations of speed-frequency couplings. **B**. Mean frequency profile of a hippocampal θ-oscillon, left-shifted by 300 ms (right scale), vs. the mean frequency of a hippocampal slow-γ oscillon, dark lilac, right-shifted by 500 ms (left scale), shown with the rat's speed profile.

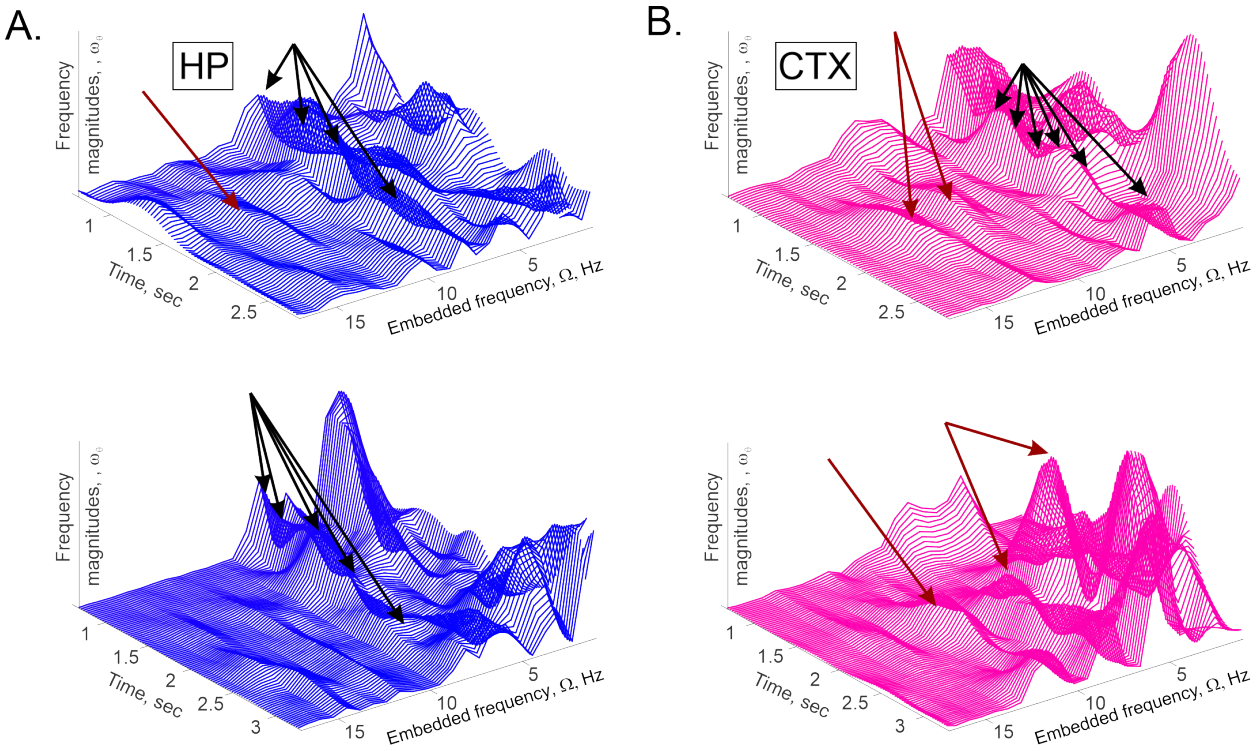

Fig. S5. **Additional examples** of hippocampal (left column) and cortical (right column) W-spectrograms, illustrating the embedded frequency dynamics for the θ-oscillons. Dark red arrows point at the appearances of isolated peaks and the black arrows point at the "seedbeds" of peaks recurring at the same frequency.

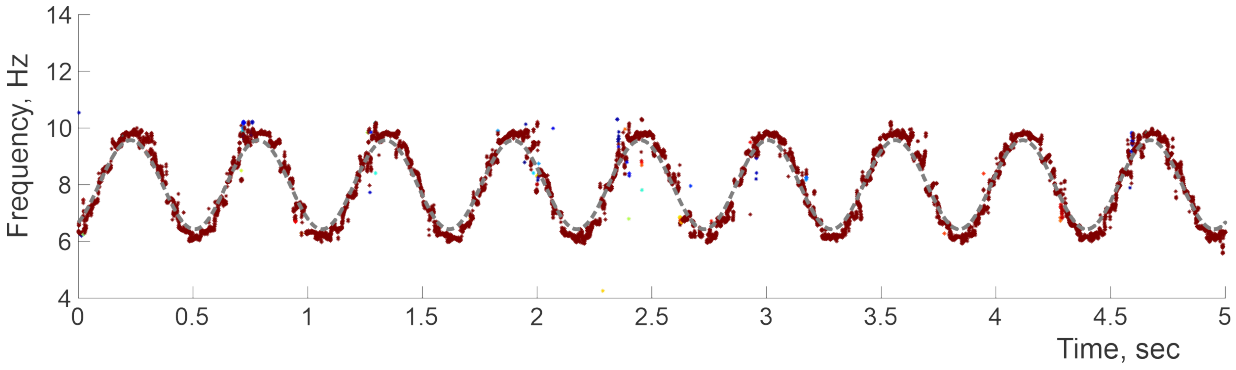

Fig. S6. **Solitary spectral wave**, used to simulate the oscillatory model (5) with a single modulating frequency, $\Omega_1/2\pi \approx 1.8$ Hz, oscillating around the mean $\nu_0 = 8$ Hz with the magnitude $\nu_1 \approx 2$ Hz (dashed gray line in the foreground). Dots represent the instantaneous DPT stable frequencies, colored according to their respective amplitudes. Physiological spectral waves shown on Figs 1 and 3 contain more than one frequency-modulating harmonic.

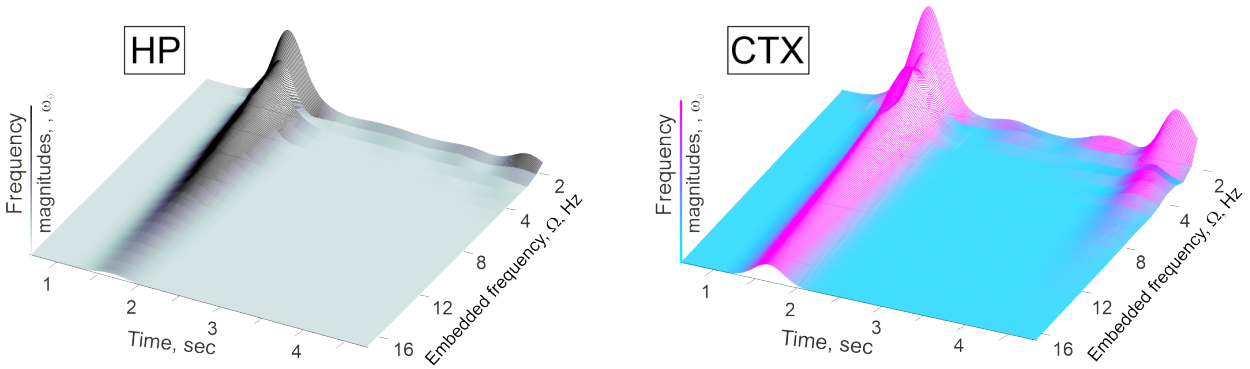

Fig. S7. **Welch spectrograms of Fourier instantaneous frequencies** (solid black line on the Fig. 3B) built for the hippocampal (left) and cortical (right) spectral-θ-waves, capture major frequency "splashes" at about 1.7 sec and 4.67 sec, but do not resolve rapid modulations of θ-frequency in-between, compare to Fig. S5.

B. Mathematical supplement

Fourier approach views signals as superpositions of harmonic waves. To evaluate their amplitudes, $2N$ data values, $\bar{\ell}_k = \{\ell_{k,1}, \ell_{k,2}, \ldots, \ell_{k,2N}\}$, centered around a discrete moment t_k, are convolved with a set of $2N$ discrete harmonics, $e^{i\pi/N}, e^{i2\pi/N}, e^{i3\pi/N}, \ldots, 1$,

$$A_{k,N} = \sum_{n=0}^{2N-1} \ell_{k,n} z_{2N}^{-n}, \tag{8}$$

where $z_{2N} = e^{i\pi/N}$. The longer is the sample set, the more precise is the spectral decomposition (8). Specifically, if the original signal is a superposition of N_P oscillators,

$$\ell(t) = \sum_{p=1}^{P} a_p e^{i2\pi(\nu_p t + \varphi_p)}, \tag{9}$$

with the amplitudes a_p, frequencies ν_p, and phases $2\pi\varphi_p$, sampled at discrete times $t_k = k\sigma$, then the Fourier amplitudes computed for a large number of data points are

$$A_{k,l} = \sum_k \ell(t_k) z_{2N}^{-k} = \sum_p \frac{a_p}{1 - z_l e^{i2\pi(\nu_p\sigma + \varphi_p)}} = \sum_p \frac{a_p}{1 - e^{i2\pi(\nu_p\sigma + \varphi_p - l/N)}}. \tag{10}$$

The closer a particular frequency $\nu_p\sigma + \varphi_p + i0$ is to a l/N, the higher is the amplitude $A_{k,l}$ of the corresponding harmonic. The segment selected for the analyses is then shifted, $\bar{\ell}_k \to \bar{\ell}_{k+1}$, yielding the next value of the amplitude, $A_{k+1,l}$, and so forth, over the entire signal span [80].

If the signal also contains noise,

$$\ell(t) = \sum_{p=1}^{P} a_p e^{i2\pi(\nu_p t + \varphi_p)} + \xi(t),$$

then the Fourier peaks broaden and their heights reduce [81]. Similar effects appear if the signal is nonstationary, e.g., if the frequencies ν_p change with time, since it becomes more difficult to match both the temporal and frequency details [7, 71, 79]. Indeed, resolving a spectral structure X that lasts over a period T_X, requires using time resolution, ΔT, shorter than T_X [6]. On the other hand, the frequency resolution, $\Delta\nu$, should be smaller than the X's spectral size. The problem is that improving the temporal resolution (lowering ΔT) reduces the number of data points caught into the sliding window, which then lowers the frequency resolution, $\Delta\nu = 1/\Delta T$, which limits the precision of the method altogether.

For example, the characteristic amplitude of the spectral waves shown on Fig. 1C and Fig. 3A is about $\Delta\nu \approx 7 - 12$ Hz, which, at the Nyquist frequency $S = 4$ kHz, requires at least $N = 600$ discrete harmonics, i.e., $N = 600$ data points per sliding window, that can be acquired over $\Delta T = N/S = 150$ ms. On the other hand, the characteristic period of the spectral waves is about $T_\theta \sim 50 - 100$ ms, i.e., in order to resolve the raising and the lowering phases of the spectral wave, ΔT should be less than 50 ms. Thus, the temporal and the frequency resolutions work against each other and leave certain details of X unresolved.

Discrete Padé Transform (DPT) approach is based on adapting the frequencies $\nu_1, \nu_2, \ldots, \nu_N$ according to the signal's structure, without restricting them to a regular "frequency grid" as in

(8) [8–10]. First, the discrete variable z_{2N} in (8) and (9) is replaced with a generic, continuous complex variable z, thus turning the sum (9) into a z-transform of the data series,

$$S(z) = \sum_{n=1}^{\infty} s_n z^{-n}. \tag{11}$$

The function (11) is then approximated by a ratio of two polynomials,

$$S_N(z) = P_{N-1}(z)/Q_N(z),$$

which constitutes the N-th order Padé approximation, $S(z) = S_N(z) + o(z^{2N})$ [82] (hence the name of the method [11]). As shown in [8, 9], the poles of $S_N(z)$, i.e., the roots of $Q_N(z)$, capture the spectral structure of the signal $\ell(t)$, similarly to the Fourier transform (10). Specifically, for the signal (9) one gets a rational function of degree $(N_P - 1)/N_P$,

$$S(z) = \sum_k s(t_k) z^k = \sum_p \frac{a_p e^{i\varphi_p}}{1 - z e^{i2\pi\nu_p\sigma}},$$

with the poles

$$z_p = e^{-i2\pi\nu_p\sigma},$$

and their residues defining the individual frequencies, ν_p, the amplitudes, a_p, and the phases, φ_p, of the corresponding oscillators.

If the signal contains a stochastic component $\xi(t)$, then the discretized time series are "noisy," $s_n = r_n + \xi_n$, and the generating function $S(z)$ acquires an "irregular" part

$$\Xi(z) = \sum_{n=0}^{\infty} \xi_n z^{-n}.$$

As it turns out, the poles of the Padé approximant to $\Xi(z)$ concentrate around the unit circle in the complex plane [63] and pair up with its roots, forming the so-called Froissart doublets [64, 65, 83, 84]. A typical pole-zero distance in the complex plane is smaller than $10^{-6} - 10^{-7}$ in the standard Euclidean metric, which allows detecting the Froissart doublets numerically. Additionally, these doublets are highly sensitive to the parameter changes, e.g., to sliding window size, whereas the unpaired poles of (10) remain stable and isolated. These differences allow delineating the LFP's noise component from the oscillations encoded by the stable poles [8, 9].

Data analyses. The mean amplitudes of the LFP time series was normalized to $\bar{\ell}(t) = 2$, with small amount of noise, $\delta\xi \approx 0.01\%$ of the total amplitude, added for numerical stability. The signal was then filtered into $1 \le f \le 60$ Hz band. The original sampling rate, $S = 8$ kHz, was interpolated to 36 kHz to improve the low-frequency spectral wave reconstruction. We then produced $2 - 3$ times undersampled sub-series, which were used for independent estimations of the regular frequencies. The sliding window width varied between $n_\varpi = 100$ to $n_\varpi = 200$ (for each undersampled subseries), which yields Padé approximants of orders $N = 50 - 200$. At the interpolated frequency, this corresponds to $T_\varpi = 8$ ms to $T_\varpi = 50$ ms time windows. To ensure maximal contiguity of the spectral waves, windows were shifted by one data point. These results remain stable under parameter variations, e.g., changes of the sliding window width [11]. The unstable frequencies were identified by detecting the Froissart doublets, with the critical pole-zero distance $d_F = 10^{-6}$ [8–11].

Welch transform allows estimating power spectra in transient signals [45]. Standard power spectra are evaluated by performing the discrete Fourier transform of the entire signal and computing the squared magnitude of the result. In Welch's approach, the signal is first split into a large number of highly overlapping shorter segments, and then the power spectrum of each segment is evaluated independently.

The power peaks obtained from a particular data segment thus mark the most prominent frequencies appearing over the corresponding time interval. Arranging such power profiles next to each other in natural order, one gets three-dimensional W-spectrograms illustrated on Fig. S8. By construction, the lateral sections of W-spectrograms are the instantaneous power—frequency profiles, whereas the longitudinal sections show the peaks' dynamics, that highlight the evolution of the corresponding embedded frequencies, $\Omega_{\theta,i}$.

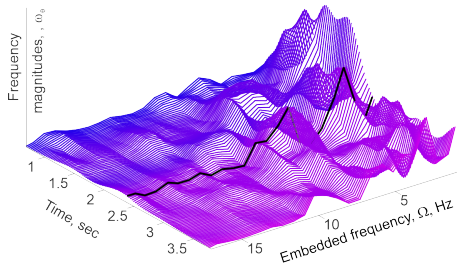

Fig. S8. **Welch spectrogram** of a hippocampal spectral wave. The black line shows power profile computed for a particular 600 ms long segment, centered at 2.4 sec. The select profile shows two peaks, which, over time, change their heights and positions, revealing the dynamic frequency landscape.

Spectral waves. Since the poles are computed independently at each time step, based on a finite number of data points, the patterns of reconstructed frequencies contain gaps and irregularities. To capture the underlying continuous physical processes, we interpolated the "raw" spectral traces over uniformly spaced time points and used Welch transform to analyze the embedded frequencies. The mean frequency was evaluated as the spectral waves' moving mean, over periods comparable with largest undulation span ~ 200 ms. All computations were performed in MATLAB.

Coupling between speed and the embedded frequencies (the dependence (4)) was obtained by evaluating the height of peaks on W-spectrogram at consecutive moments of time and comparing them to the ongoing speed values. Computations were made for peaks exceeding 20% of the mean height of W-spectrograms, for each analyzed data segment. All computations were performed in MATLAB.

Kuramoto model describes a network of oscillators, coupled via the equation

$$\dot{\varphi}_k = 2\pi\nu_k + \frac{\lambda}{m_k}\sum_{l=1}^{N} C_{kl}\sin\left(\varphi_l - \varphi_k\right),$$

where m_k is the valency of the oscillator ℓ_k, and C_{kl} is the adjacency matrix

$$C_{kl} = \begin{cases} 1 \text{ if } \ell_k \text{ is connected to } \ell_l, \\ 0 \text{ otherwise,} \end{cases}$$

and m_k is the valency of the node ℓ_k. In this study, the network had scale-free connectivity. The mean field produced at the k^{th} node is

$$A_{K,k}e^{i\phi_K} = \sum_{l=1}^{N} C_{kl}e^{i\varphi_l}. \tag{12}$$

Multiplying both sides of (12) by $e^{-i\varphi_k}$ and taking the imaginary part, one recovers the equation (7), which highlights the mean field dynamics.